

Numerical Analysis of Tip Leakage Flow Field in a Transonic Axial Compressor Rotor

Kazutoyo YAMADA^{*1}, Masato FURUKAWA^{*2}, Masahiro INOUE^{*2}, and Ken-ichi FUNAZAKI^{*1}

^{*1} Department of Mechanical Engineering
Iwate University

4-3-5 Ueda, Morioka, Iwate 020-8551, Japan

Phone: +81-19-621-6424, FAX: +81-19-621-6424, E-mail: yamada@iwate-u.ac.jp

^{*2} Kyushu University

ABSTRACT

Tip leakage flow field in a transonic axial compressor rotor, NASA Rotor 37, were investigated by large-scale numerical simulations. Unsteady three-dimensional flow simulations were conducted by solving the compressible RANS (Reynolds-averaged Navier-Stokes) equations with $k-\omega$ turbulence model using an implicit high-resolution upwind scheme based on a TVD formulation. Vortical flow structures were focused on in order to investigate the tip leakage flow field in detail. At the tip leakage flow field in the rotor passage, the tip leakage vortex interacts with the shock wave formed upstream of the leading edge of rotor blade. This interaction has a great influence on the loss at the tip flow region. In addition, the simulation shows that the vortex breakdown occurs in the tip leakage vortex at near-stall condition due to this interaction, generating a large blockage effect near the tip in the rotor passage enough to trigger the stall of compressor. The breakdown leads to the unsteadiness in the tip leakage vortex, which causes the periodical fluctuations of blade torque, playing a major role in the unsteady phenomena in the tip leakage flow field.

INTRODUCTION

It is well known that the tip leakage flow is very important flow phenomena for decreasing the aerodynamic performance and efficiency of compressors. The shear layer due to the tip leakage flow rolls up inside the rotor passage to yield a large-scale streamwise slender vortex, a so-called 'tip leakage vortex'. In a transonic compressor rotor, the tip leakage vortex interacts with the endwall boundary layer and shock wave in the passage, which forms the complicated flow field near the tip region. It is difficult to clarify these flow phenomena in only an experimental technique because they occur in the very small region near the tip in the rotor passage. Therefore, a number of numerical studies were performed to investigate the tip flow field in a transonic compressor rotor (Copenhaver et al. [1996], Chima [1998], Gerolymos et

al. [1999], and Hoeger et al. [1999]). The effects of tip clearance on the performance of a transonic compressor rotor were investigated by Adamczyk et al. [1993]. They indicated that the low-energy fluid appears along the casing due to the interaction of the tip clearance vortex and the rotor passage shock, and showed that an increased flow range was achieved without the tip clearance due to the absence of the vortex/shock interaction. Suder and Celestina [1996] reports that the interaction between the tip leakage vortex and the rotor passage shock generates a larger region of high blockage near the tip in the passage as the rotor loadings is increased. In addition, it was indicated that the blockage effect due to the vortex/shock interaction leads to high incidence angles at the tip, which may play a role in bringing about tip stall of the rotor. However, in spite of a number of such efforts details of the blockage in the tip region of transonic compressor rotor have not been revealed yet.

The purpose of the present work is to elucidate the tip flow field in a transonic axial compressor rotor, and to predict the blockage in the tip region. The tip flow fields in the transonic rotor at near peak efficiency condition and near-stall condition have been investigated by unsteady three-dimensional Navier-Stokes flow simulations based on an implicit high-resolution upwind scheme using the TVD formulation and by a method of identifying vortex structures based on the critical-point theory.

TEST COMPRESSOR ROTOR

Transonic axial compressor rotor, NASA Rotor 37, was used in the present work. The rotor was originally designed as an inlet rotor for a core compressor and tested at NASA Lewis Research Center in the late 1970's. The specification of the rotor is summarized in Table 1. The rotor design pressure ratio is 2.106 at a mass flow of 20.19kg/s. The inlet relative Mach number is 1.13 at the hub and 1.48 at the tip at the design speed of 454m/s (17,188.7rpm). The rotor has 36 blades with a hub-tip ratio of 0.7, an aspect ratio of 1.19, and a tip solidity of 1.288. The tip clearance is 0.400mm. Details of the rotor aerodynamic design were reported by Reid and Moore [1978]. Figure 1 shows the location measured using aerodynamic probes and laser anemom-

Table 1 Design specification of test compressor

Blade number	36
Radius of tip at leading edge	252mm
Aspect ratio	1.19
Solidity at tip	1.288
Tip clearance	0.400mm(0.51%Span)
Hub-tip ratio	0.7
at design	
Tip speed	454m/s(17,188.7rpm)
Total Pressure rise ratio	2.106
Massflow	20.19kg/s
Choke massflow	20.93kg/s

Station	Z(mm)*	Span	%Span
1	-41.9	1	30
2	20%chord	2	50
3	45.7	3	90
4	10.67	4	95

*Z=0 at intersection of hub and leading edge

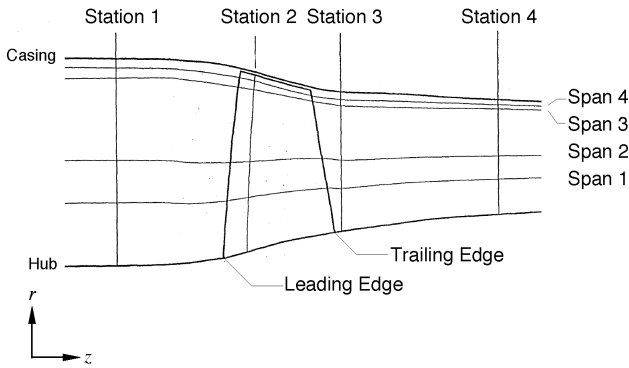


Fig. 1 Locations measured in experiment

eter system, where radial distributions of static and total pressure, and total temperature are obtained as well as velocity distributions at some blade-to-blade planes.

NUMERICAL ANALYSIS METHOD

Numerical Scheme

Unsteady three-dimensional flow simulations were performed by solving the compressible Navier-Stokes equations using an unfactored implicit upwind relaxation scheme with inner iterations (Furukawa et al. [1992]; Inoue and Furukawa [1994]). The numerical method used in the present flow solver is outlined in the following.

The three-dimensional Reynolds-averaged Navier-Stokes equations were discretized in space using a cell-centered finite volume formulation and in time using the Euler implicit method. The inviscid fluxes were evaluated by a high-resolution upwind scheme based on a TVD formulation (Furukawa et al. [1991]), where a Roe's approximate Riemann solver of Chakravarthy [1986] and a third-order accurate MUSCL approach of Anderson et al. [1986] with the Van Albada limiter were implemented. The viscous fluxes were determined in a central differencing manner with Gauss's theorem. The $k-\omega$ turbulence model (Wilcox [1988]) was employed to estimate the eddy viscosity. Simultaneous equations linearized in time were solved by a point Gauss-Seidel relaxation method using no approximate factorization (Furukawa et al. [1992], [1995]). To obtain a time-accurate solu-

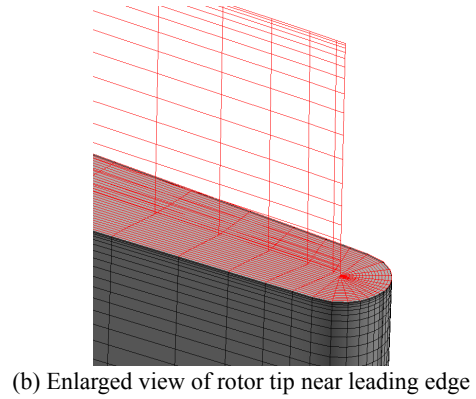
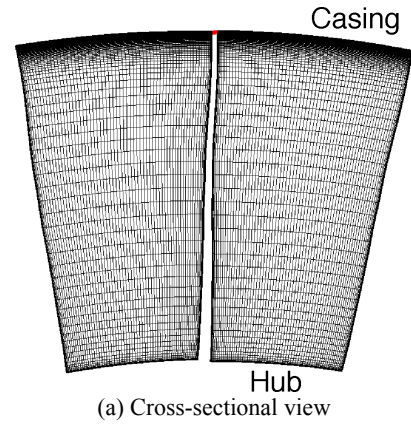


Fig. 2 Computational grid

tion, inner iterations, so-called Newton iterations, were introduced at each time step according to Chakravarthy [1984]. The scheme was kept second-order accurate in time by applying the three-point-backward difference approximation to the temporal derivative (Inoue and Furukawa [1994]). It should be noted that the present implicit scheme with the relaxation method has no factorization error, thus being stable up to much larger size of time step than implicit schemes with approximate factorization. For the unsteady flow simulations presented in this paper, nine inner iterations were performed at each time step, and a nondimensional time step size normalized by the rotor tip radius and the inlet sound speed was set to 0.0001. More than 1,300 time steps are included in the interval of time taken for a rotor blade to pass through one pitch.

Computational Grid

The computational grid used in the present work is shown in Fig. 2. The composite-grid system was employed to the present simulation. A computational domain was divided into two zones. One zone was a main flow region outside the blade tip clearance, and the other was the tip clearance region. A structured H-type grid was generated in the main flow region, while in the tip clearance region a structured O-type grid was generated. The main grid consisted of 160 cells in the streamwise direction (83 cells on the blade), 105 cells in the spanwise direction, and 78 cells in the pitchwise direction. In order to capture the tip leakage flow field accurately, the grid resolution near the rotor tip was kept high as shown in Fig. 2(a). The grid embedded in the blade tip

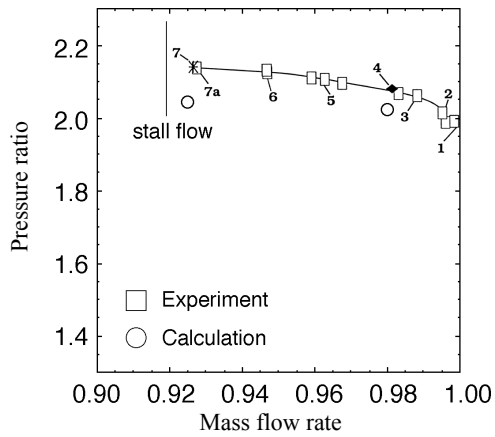


Fig.3 Total pressure ratio characteristics of rotor

clearance consisted of $83 \times 20 \times 32$ cells in the chordwise, spanwise and pitchwise directions, respectively. The whole grid system had 1,363,520 cells. The grid dependency was investigated in advance. As a result, it was confirmed that the present grid had grid convergence. The ratio of the minimum grid spacing on solid walls to the blade tip chord length was under 5×10^{-5} to evaluate the viscous fluxes at the walls by applying the no-slip and adiabatic conditions with no wall function method. This minimum grid spacing gave $y^+ < 1$ at the walls. The experimental data measured at Station 1 shown in Fig. 1 were used for the inlet boundary condition of the present calculation.

Identification of Vortex Structures

The identification of vortex is very useful in understanding the complicated flow fields like those in turbomachinery. It is hard to have a clear grasp of the tip leakage flow field in compressor rotor by conventional flow visualization techniques such as particle traces, contour plots, secondary vector plots and so on. It is essential and key point to identify the vortex structure for the purpose of revealing the unsteady flow phenomena near rotor tip in the transonic axial compressor rotor.

A trajectory of the vortex core is identified by a semi-analytic method developed by Sawada [1995]. In his method, assuming that a local velocity field can be linearly parametrized in a tetrahedral computational cell, streamline equations become integrable analytically for the cell, and as a result the obtained streamline expression provides a possible vortex center line in the cell. In the present study, each hexahedral computational cell is divided into five tetrahedra to apply Sawada's method. The computational cell crossed by the vortex center line is defined as a fraction of the vortex core. The value of unity is given at each vertex of the cells crossed by the vortex center, and zero at the vertexes of the other cells. An iso-surface of the adjusted value is drawn to represent the whole vortex core structure.

Validity of Numerical Simulation

In the present work, the numerical simulations were conducted to investigate the tip flow fields in the rotor at two operating

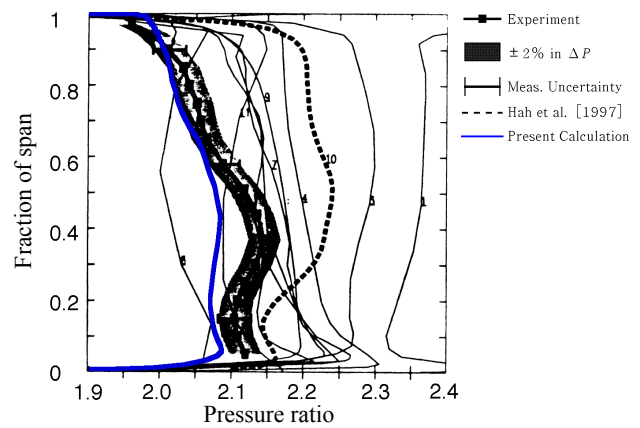


Fig.4 Spanwise distributions of total pressure ratio

points of near peak efficiency condition (98% mass flow rate) and near-stall condition (92.5% mass flow rate). The total pressure ratio characteristics are shown in Fig. 3. The predictions of the simulations give a little lower total pressure ratio compared to the experimental ones.

In the previous studies (Furukawa et al. [1995, 1999]), the validity of the numerical scheme has been presented by comparing numerical results with experimental ones. In Fig. 4, the spanwise distributions of total pressure ratio are compared between computational and experimental results in order to demonstrate the validity of numerical simulations performed in the present study. The computed pressure ratio is a little lower than the experimental one, especially around the mid-span. It probably seems to be because of the coarser grid resolution around the mid-span than that near the rotor tip. This disagreement corresponds to that in Fig. 3. However, the simulation result has a good agreement with the experimental one near the hub and the tip region. It seems to be quite good for analyzing the tip flow field in the rotor. In Figs. 5 and 6, the comparisons between numerical and experimental results are shown at near peak efficiency condition and near-stall condition, respectively. In these figures, the axial velocity distributions are represented at Station 2, which is the plane perpendicular to the axis as shown in Fig. 1, and are compared only near the casing. In Fig. 5, it is found that the shock wave appears near the midpitch across this plane, and at the same time the low-energy fluid accumulates just near the casing on the pressure side of the shock wave. This fact is confirmed for the both of numerical and experimental results. At near-stall condition, the accumulation of the low-energy fluid near the casing becomes larger than that at near peak efficiency condition, as seen in the both results in Fig. 6. It is found that the present simulations predicted exactly these flow phenomena at the tip flow field in the rotor passage.

RESULTS AND DISCUSSION

Flow Field at Near Peak Efficiency Condition

The flow fields at the near peak efficiency condition are shown in Fig. 7. Experimental result measured by the laser anemometer

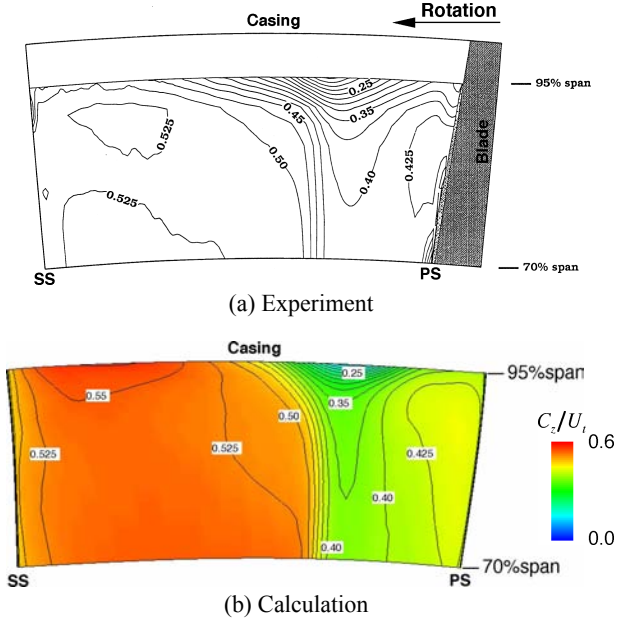


Fig.5 Axial velocity distributions at Station 2 at near peak efficiency condition

shows a relative Mach number contour at 95% span in Fig. 7(a). Fig. 7(b) shows numerical result with a relative Mach number contour at 95% span and vortex cores in the rotor identified according to the method above-mentioned. Vortex cores were colored with the relative Mach number (the upper passage) and the normalized helicity H_n (the bottom passage) defined as follows:

$$H_n = \frac{\vec{\xi} \cdot \vec{w}}{|\vec{\xi}| |\vec{w}|} \quad (1)$$

where $\vec{\xi}$ and \vec{w} denote vectors of the absolute vorticity and the relative flow velocity, respectively. The magnitude of the normalized helicity H_n takes the value of unity anywhere the streamwise vortex is present and it can assess the nature of vortex quantitatively, in any case the vorticity decays. As seen in the relative Mach number contours in Fig. 7, the shock wave appears near the leading edge of rotor blade, and interacting with the suction surface of neighboring blade. Vortex cores of almost -1 in the normalized helicity are observed near the tip flow field in rotor, implying the presence of streamwise vortex, which represents tip leakage vortex rolling up from the leading edge of rotor. It is found that the tip leakage vortex interacts with the shock wave in the rotor passage, abruptly being decelerated downstream of the shock as seen in the relative Mach number distribution on the vortex core. This leads to the expansion of tip leakage vortex, and finally yielding the decelerated region just downstream of the shock wave near the tip, which is also found in the experiment.

Breakdown of Tip Leakage Vortex at Near-Stall Condition

At near-stall condition, the unsteady simulation was conducted to investigate the unsteady tip flow field in the rotor. Figure 8

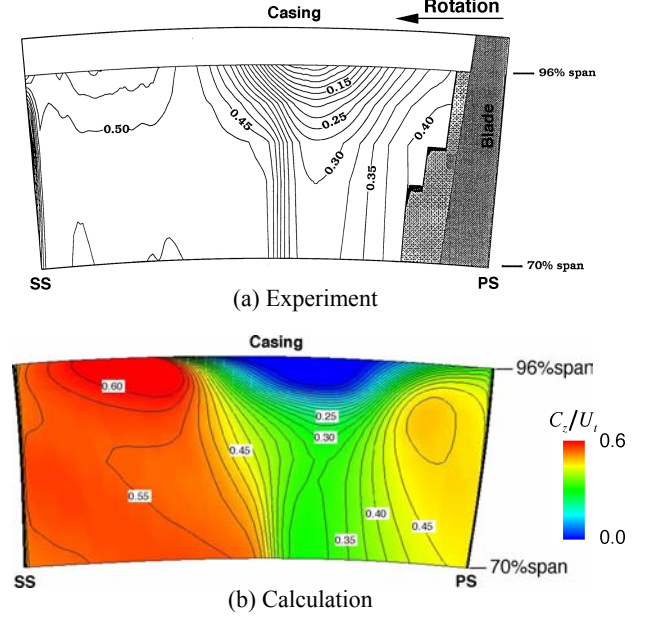


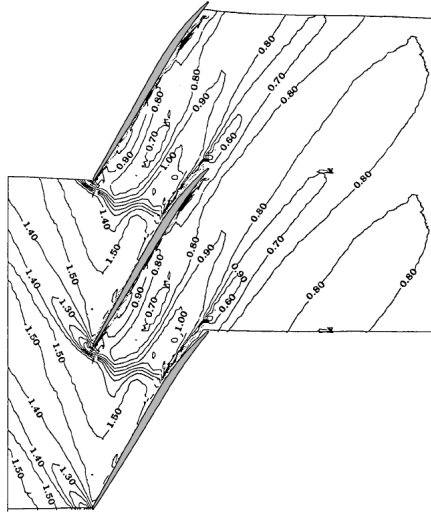
Fig.6 Axial velocity distributions at Station 2 at near-stall condition

shows the time history of blade torque coefficient C_t , which is defined as follows:

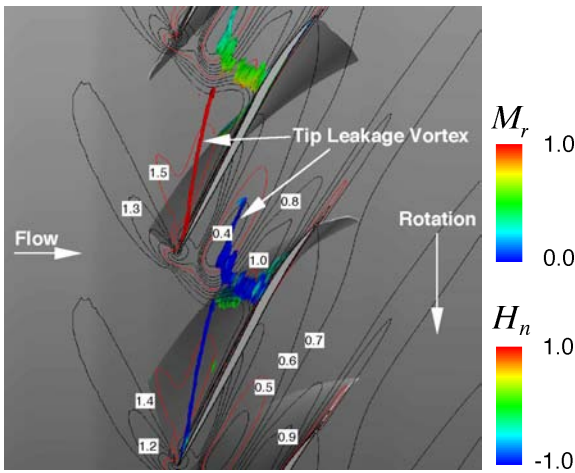
$$C_t = \frac{T}{\rho U_t^2 r_t^2 / 2} \quad (2)$$

where ρ , U_t , r_t , and T are the density, the blade tip speed, the blade tip radius, and the blade torque, respectively. Time-averaged flow field, which was obtained to average the unsteady numerical results over nearly two nondimensional times after passing the transitional period of calculation as shown in Fig. 8, was investigated in this section. Figure 9 describes the time-averaged flow field in the rotor at near-stall condition. Just as shown in Fig. 7, the relative Mach number contour at 95% span and vortex cores identified in the rotor are illustrated in this figure, where the vortex cores were colored with the relative Mach number (the upper passage) and the normalized helicity H_n (the bottom passage). Although the tip leakage vortex appears in the rotor, downstream of the shock wave it has a positive value of the normalized helicity contrary to that at the origin of its rolling up near the leading edge. In addition, it is found that the relative Mach number of tip leakage vortex is decelerated to be almost zero downstream of the shock wave, where there might be the recirculation region, and the region with the low-energy fluid downstream of the shock expands in the rotor passage drastically. These phenomena mean that the tip leakage vortex has experienced a significant change in its streamwise slender vortex structure. In Fig. 10, distributions of absolute vorticity coefficient ξ_n in the rotor passage are shown on the crossflow planes nearly perpendicular to the tip leakage vortex. At the same time, the tip leakage streamlines are shown in this figure. The absolute vorticity coefficient ξ_n is defined as follows:

$$\xi_n = \frac{|\vec{\xi}|}{2\omega} \quad (3)$$



(a) Experiment



(b) Calculation

Fig.7 Tip flow field at near efficiency condition: relative Mach number contour at 95% span and (b) vortex cores colored with relative Mach number (upper passage) and normalized helicity (bottom passage)

where ω is the magnitude of the rotor angular velocity. As seen on the plane I upstream of the shock wave, the tip leakage vortex has a concentrated absolute vorticity before interacting with the shock wave. However, at the plane II downstream of the shock wave the region with a concentrated absolute vorticity has expanded abruptly. This applies to the tip leakage streamlines, too. Namely, these mean the sudden expansion of the tip leakage vortex. In addition, there is no concentrated absolute vorticity at the center of the tip leakage vortex at the plane II, as seen in Fig. 10. These flow phenomena above-mentioned in the tip leakage vortex downstream of the shock: the stagnation (recirculation) region, the unexpected expansion of the tip leakage vortex, and the lack of concentrated absolute vorticity in the vortex center, correspond to some features of ‘vortex breakdown’ (Leibovich [1978], Deley [1994]). It is well known that vortex breakdown occur in leading edge vortices over delta wings, swirling jets in combustion chambers, and swirling flows in draft tubes of hydraulic turbines. Recently, it has been observed even in turbomachineries: a low-speed axial compressor rotor (Furukawa et al.

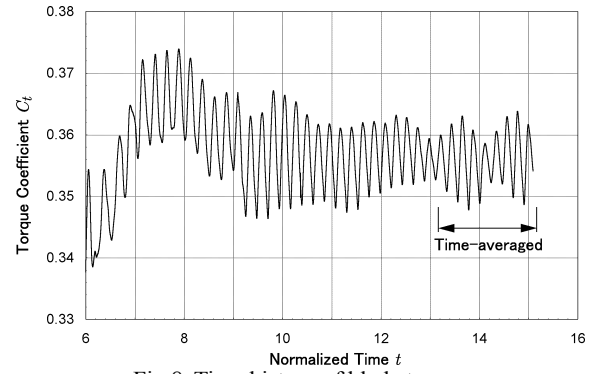


Fig.8 Time history of blade torque

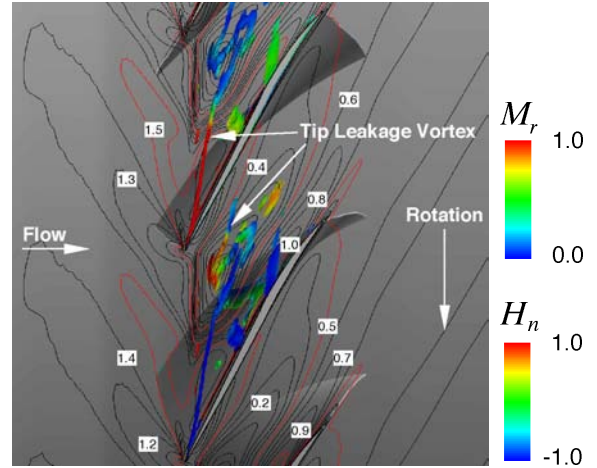


Fig.9 Tip flow field at near-stall condition: relative Mach number contour at 95% span and vortex cores colored with relative Mach number (upper passage) and normalized helicity (bottom passage)

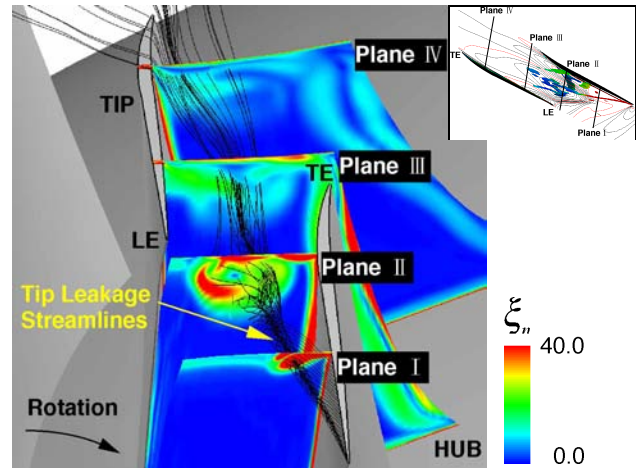


Fig.10 Absolute vorticity distributions on crossflow planes at near-stall condition

[1999]) and a transonic compressor rotor (Schlechtriem et al. [1997]). Vortex breakdown represents an abrupt change in the vortex core structure, but its stability criterion is not fully elucidated yet. It has been found, however, that there are two types in vortex breakdown: bubble and spiral types, vortex breakdown is influenced by the adverse pressure gradient in streamwise direction and the swirl intensity of the vortex, and has some features such as a reversed flow region, a sudden expansion of the vortex, and large-scale flow fluctuations. Therefore, the vortex break-

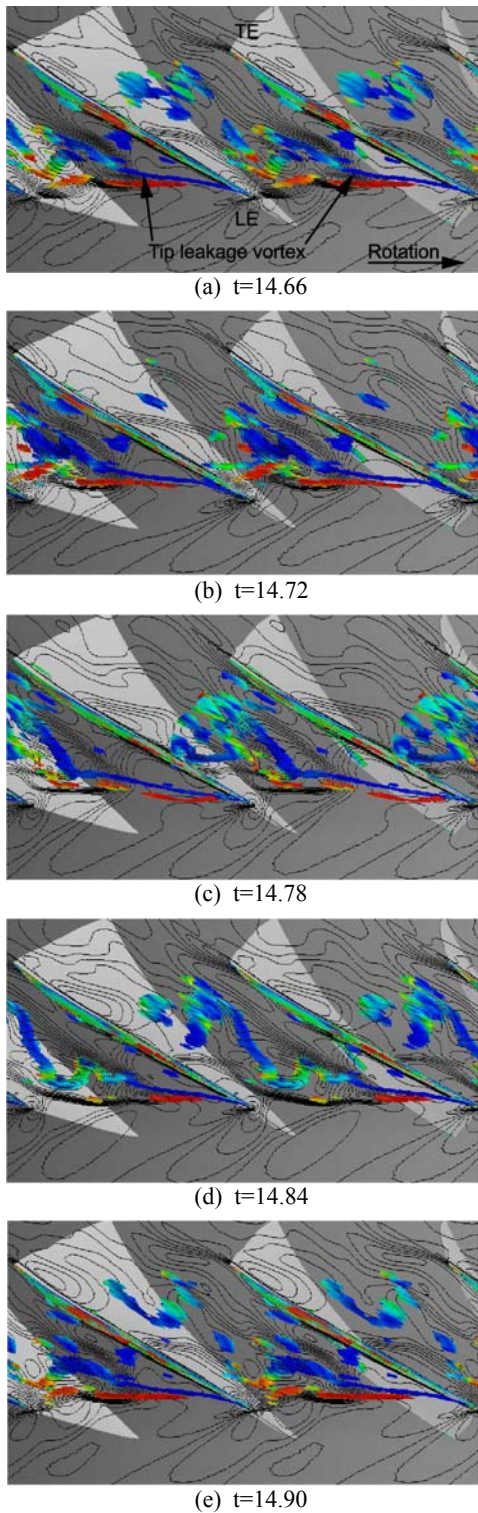


Fig.11 Unsteady behavior of relative Mach number contour at 95% span and vortex cores colored with normalized helicity at near-stall condition

down can be caused by the shock/vortex interaction, which has been investigated by Smart et al. [1997] in detail. As a whole, the breakdown of the tip leakage vortex seems to be brought about due to the interaction of the tip leakage vortex with the shock wave when the swirl intensity of the tip leakage vortex increasing with the blade loading at near-stall condition. In this way, it is found that the tip leakage vortex breakdown leads to the large

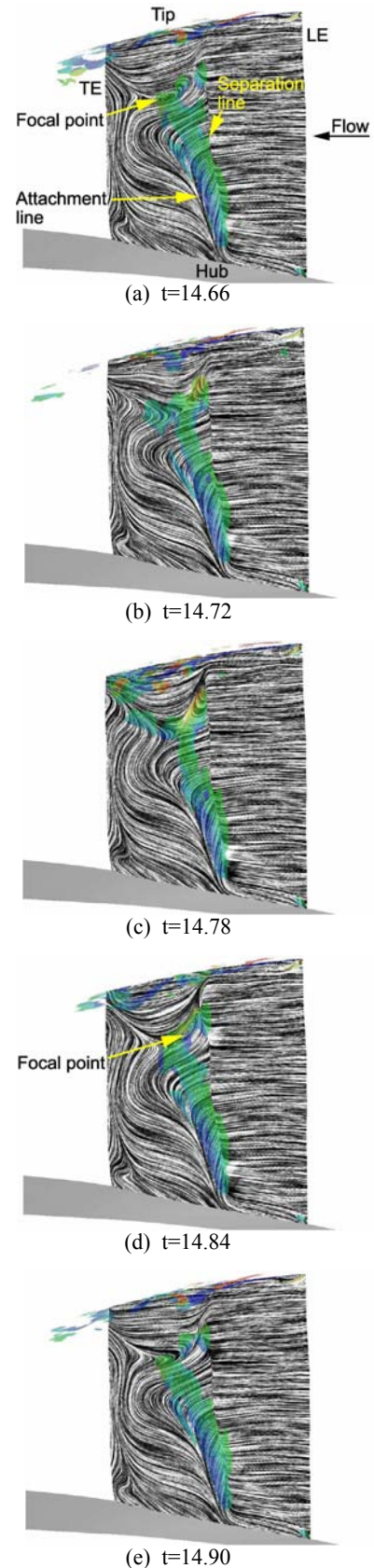


Fig. 12 Unsteady behavior of limiting streamlines on blade suction surface at near-stall condition

blockage effect near the tip in the rotor passage at near-stall condition.

Unsteady Behavior of Tip Leakage Vortex Due to Its Breakdown

As above-mentioned the vortex breakdown has a large-scale unsteady nature and the unsteady flow behaviors due to the breakdown of the tip leakage vortex are investigated in this section. Figs. 11 and 12 show the unsteady flow field in the rotor at near-stall condition. Some instantaneous flow fields in about one cycle of the periodic fluctuation of the blade torque in Fig. 8 are shown in these figure.

The unsteady behaviors of the relative Mach number contour at 95% span and vortex cores colored with the normalized helicity are shown in Fig. 11. It is found that the breakdown of the tip leakage vortex is spiral-type and the tip leakage vortex fluctuates with time in the rotor passage. The tip leakage vortex twists and turns violently in the pitchwise direction to interact with the pressure surface of the adjacent blade. At the same time, the low-energy fluid downstream of the shock wave near the tip fluctuates with the periodical behavior of the tip leakage vortex, as seen by the relative Mach number contour at 95% span. The tip leakage vortex decays in the aft part of the rotor passage soon after impinging on the pressure surface near the leading edge. This cyclic interaction of the part of the tip leakage vortex with the adjacent blade corresponds to the fluctuation of the blade torque as shown in Fig. 8.

Fig. 12 shows the variation of the limiting streamlines on the suction surface using LIC visualization technique (Cabral et al. [1993]). It is found that there are the bifurcation lines of separation and attachment lines near mid-chord due to the interaction of the shock wave. The location and type of these bifurcation lines do not vary with time near the hub. The topology of the limiting streamlines, however, changes with time in the outward radius from 80% span, and the focal-type critical point, which indicates three-dimensional attachment point, appears just downstream of the shock at $t=14.66$ and $t=14.84$. By such means, it should be considered that three-dimensional flow field is formed near the tip contrary to two-dimensional flow field near the hub. It is evident that the variation of limiting streamlines and three-dimensional flow patterns near the tip are caused by the tip leakage vortex breakdown.

Effects of Tip Leakage Vortex Breakdown

Figure 13 shows the distributions of total pressure loss coefficient ζ_p on the meridional planes near the midpitch of the rotor passage at near peak efficiency condition and near-stall condition. The total pressure loss coefficient ζ_p is defined as

$$\zeta_p = \frac{\omega(r c_\theta - r_1 c_{\theta 1}) - (P - P_1)/\rho}{U_t^2/2} \quad (4)$$

where r is the radius from the axis of rotation, c_θ is the absolute tangential velocity component, P is the total pressure, and subscript of 1 denotes the rotor inlet. The interaction between the tip leakage vortex and the shock wave resulted in the high loss at the tip in the rotor passage. Its influence nearly reaches the outer 10% span at near peak efficiency condition. The similar results

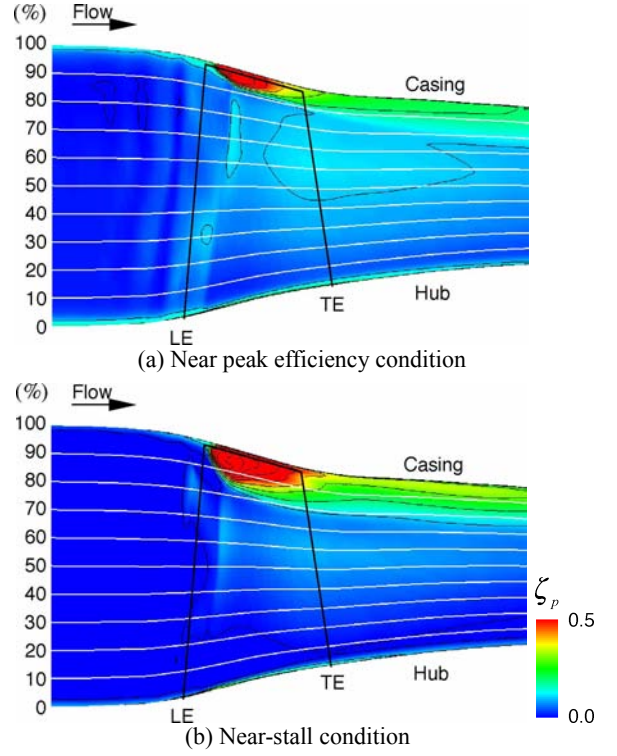


Fig.13 Total pressure loss distributions on meridional plane near midpitch

are described by Suder and Celestina [1996]. At near-stall condition the high loss region near the tip significantly extends over the outer 20% span due to the breakdown of tip leakage vortex, as seen in Fig 13(b). The high loss region corresponds to the blockage region due to the accumulation of the low-energy fluid, and the large blockage effect near the tip might finally give rise to the stall of compressor.

Figure 14 shows the breakdown limit curve for NSVI (normal shock wave/vortex interaction) introduced by Smart et al. [1997]. The curve shown in this figure analytically predicts the presence of breakdown of the streamwise slender vortex caused by the interaction with the normal shock wave, and is presented with respect to the freestream Mach number and the swirl ratio τ upstream of the shock. The swirl ratio τ is defined as follows:

$$\tau = \frac{\Lambda_{\max}}{V_a} \quad (5)$$

where Λ_{\max} is the maximum of swirl velocity component in vortex core, and V_a is the velocity component along the vortex axis direction at the vortex axis. The present numerical simulations (circle symbols) represent as good correlation with the NSVI breakdown limit as a number of shock/vortex interaction experiments. The simulation result at near-stall condition is close to the curve, which means that the breakdown of the tip leakage vortex has occurred just before the stall point.

These flow phenomena above-mentioned due to the tip leakage vortex breakdown in the tip flow field at near-stall condition: the unsteady behavior of tip leakage vortex and the extreme extension of high loss region and blockage effect, seem to imply the

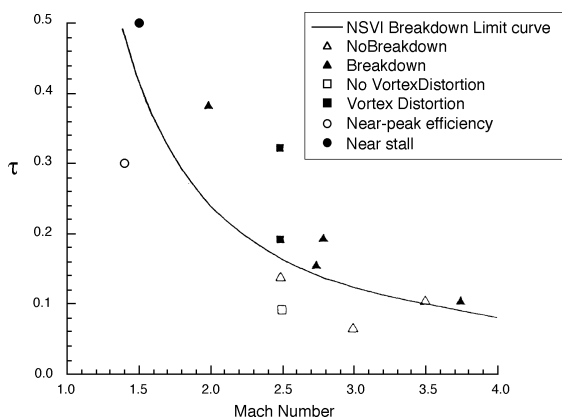


Fig.14 Breakdown limit curve for normal shock wave/vortex interaction (NSVI)

relationship between the breakdown of tip leakage vortex and the onset of the stall of compressor rotor.

CONCLUSION

Unsteady three-dimensional Navier-Stokes flow simulations based on the high-resolution upwind scheme using the TVD formulation were conducted in order to investigate the tip flow field in a transonic axial compressor rotor. The results are summarized as follows:

- (1) Even at near peak efficiency condition the low-energy fluid appears downstream of the shock wave near the tip due to the expansion of the tip leakage vortex in interacting with the shock wave although its region is small.
- (2) At near-stall condition the breakdown of the tip leakage vortex takes place in the rotor passage just downstream of the shock because the tip leakage vortex, which has strong swirl intensity increased at near-stall condition, interacts with the shock wave.
- (3) The breakdown of the tip leakage vortex leads to not only a large blockage effect near the tip but also the unsteady flow phenomena in the rotor passage. The blockage effect extend to 20% span from the casing, which is two times as large as that at near peak efficiency condition. The periodic fluctuations of the blade torque, the low-energy fluid downstream of the shock near the tip, and limiting streamlines on the blade suction surface are caused by the unsteady behavior of the tip leakage vortex due to its breakdown.

REFERENCES

- [1] Adamczyk, J. J., Celestina, M. L., and Greitzer, E. M., 1993, "The Role of Tip Clearance in High-Speed Fan Stall," *ASME Journal of Turbomachinery*, Vol. 115, pp. 28-39.
- [2] Anderson, W. K., Thomas, J. L., and van Leer, B., 1986, "Comparison of Finite Volume Flux Vector Splittings for the Euler Equations," *AIAA Journal*, Vol. 24, No.9, pp. 1453-1460.
- [3] Cabral, B., and Leedom, C., 1993, "Imaging Vector Fields Using Line Integral Convolution," *Computer Graphics Proc. '93, ACM SIGGRAPH*, pp. 263-270.
- [4] Chakravarthy, S. R., 1984, "Relaxation Method for Unfactored Implicit Upwind Schemes," *AIAA Paper No. 84-0165*.
- [5] Chakravarthy, S. R., 1986, "The Versatility and Reliability of Euler Solvers Based on High-Accuracy TVD Formulations," *AIAA Paper No. 86-0243*.
- [6] Chima, R. V., 1998, "Calculation of Tip Clearance Effect in a Transonic Compressor Rotor," *ASME Journal of Turbomachinery*, Vol. 120, pp. 131-140.
- [7] Copenhaver, W. W., Mayhew, E. R., Hah, C., and Wadia, A. R., 1996, "The Effect of Tip Clearance on a Swept Transonic Compressor Rotor," *ASME Journal of Turbomachinery*, Vol. 118, pp. 230-239.
- [8] Deley, J. M., 1994, "Aspects of Vortex Breakdown," *Prog. Aerospace Sci.*, Vol. 30, pp. 1-59.
- [9] Furukawa, M., Yamasaki, M., and Inoue, M., 1991, "A Zonal Approach for Navier-Stokes Computations of Compressible Cascade Flow Fields Using a TVD Finite Volume Method," *ASME Journal of Turbomachinery*, Vol. 113, No.4, pp. 573-582.
- [10] Furukawa, M., Nakano, T., and Inoue, M., 1992, "Unsteady Navier-Stokes Simulation of Transonic Cascade Flow Using an Unfactored Implicit Upwind Relaxation Scheme With Inner Iterations," *ASME Journal of Turbomachinery*, Vol. 114, No.3, pp. 599-606.
- [11] Furukawa, M., Saiki, K., and Inoue, M., 1995, "Numerical Simulation of Three-Dimensional Viscous Flow in Diagonal Flow Impeller," in: *Numerical Simulations in Turbomachinery*, ASME FED-Vol. 227, 29-36.
- [12] Furukawa, M., Inoue, M., Saiki, K., and Yamada, K., 1999, "The Role of Tip Leakage Vortex Breakdown in Compressor Rotor Aerodynamics," *ASME Journal of Turbomachinery*, Vol. 121, No.3, pp. 469-480.
- [13] Furukawa, M., Saiki, K., Yamada, K., and Inoue, M., 2000, "Unsteady Flow Behavior Due to Breakdown of Tip Leakage Vortex in an Axial Compressor Rotor at Near-Stall Condition," *ASME Paper No. 2000-GT-666*, pp. 1-12.
- [14] Gerolymos, G. A., and Vallet, I., 1999, "Tip-Clearance and Secondary Flows in a Transonic Compressor Rotor," *ASME Journal of Turbomachinery*, Vol. 121, pp. 751-762.
- [15] Hoeger, M., Fritsch, G., and Bauer, D., 1999, "Numerical Simulation of the Shock-Tip Leakage Vortex Interaction in a HPC Front Stage," *ASME Journal of Turbomachinery*, Vol. 121, pp. 456-468.
- [16] Inoue, M. and Furukawa, M., 1994, "Artificial Dissipative and Upwind Schemes for Turbomachinery Blade Flow Calculation," *VKI Lecture Series No. 1994-06*.
- [17] Leibovich, S., 1978, "The Structure of Vortex Breakdown," *Annual Review of Fluid Mechanics*, Vol. 10, pp. 221-246.
- [18] Reid, L., and Moore, R. D., 1978, "Design and Overall Performance of Four Highly-Loaded, High-Speed Inlet Stages for an Advanced, High-Pressure-Ratio Core Compressor," *NASA TP-1337*.
- [19] Sawada, K., 1995, "A Convenient Visualization Method for Identifying Vortex Centers," *Trans. Japan Soc. of Aero. Space Sci.*, Vol. 38, No. 120, pp. 102-116.
- [20] Schlechtriem, S., and Lotzerich, M., 1997, "Breakdown of Tip Leakage Vortices in Compressors at Flow Conditions Close to Stall," *ASME Paper No. 97-GT-41*.
- [21] Smart, M. K., and Kalkhoran, I. M., 1997, "Flow Model for Predicting Normal Shock Wave Induced Vortex Breakdown," *AIAA Journal*, Vol. 35, No. 10, pp. 1589-1596.
- [22] Suder, K. L. and Celestina, M. L., 1996, "Experiment and Computational Investigation of the Tip Clearance Flow in a Transonic Axial Compressor Rotor," *ASME Journal of Turbomachinery*, Vol. 118, pp. 218-229.
- [23] Wilcox, D. C., 1988, "Reassessment of the Scale-Determining Equation of Advanced Turbulence Models," *AIAA Journal*, Vol. 26, No. 11, pp. 1299-1310.